Supporting Information

Unraveling hydridic-to-protonic dihydrogen bond predominance in monohydrated dodecaborate clusters

Yanrong Jiang,[#[a]] Qinqin Yuan,[#[b][e]] Wenjin Cao,[[b]] Zhubin Hu,[[a]] Yan Yang,[[a]] Cheng Zhong,[[d]] Tao Yang,[[a]] Haitao Sun,*[[a][c]] Xue-Bin Wang*[[b]] and Zhenrong Sun*[[a][c]]

a. State Key Laboratory of Precision Spectroscopy, School of Physics and Electronic Science, East China Normal University, Shanghai 200062, China. E-mail: htsun@phy.ecnu.edu.cn ; zrsun@phy.ecnu.edu.cn
b. Physical Sciences Division, Pacific Northwest National Laboratory, 902 Battelle Boulevard, P. O. Box 999, MS K8-88, Richland, Washington 99352, USA. E-mail: xuebin.wang@pnnl.gov
c. Collaborative Innovation Center of Extreme Optics, Shanxi University, Taiyuan, Shanxi 030006, China
d. College of Chemistry & Molecular Sciences, Wuhan University, Wuhan Hubei 430072, China
e. Department of Chemistry, Anhui University, Hefei, Anhui, 230601, China
† Electronic Supplementary Information (ESI) available: Spectroscopic, DFT, and additional experimental data.
# These authors contributed equally to this work.
* These authors jointly supervised this work.

Table of Contents

Experimental Procedures

Photoelectron spectroscopy. The experiments were carried out using a magnetic-bottle (MB) photoelectron spectroscopy (PES) apparatus equipped with an electrospray ionization source (ESI), a quadrupole mass spectrometer (QMS), a temperature-controlled 3D cryogenic ion trap and a time-of-flight (TOF) mass spectrometer.[1] In order to produce all desired hydrated anion clusters of $B_{12}X_{12}^{2-}\cdot H_2O$ (X = H, F, I), ~1 mM ESI solutions of inorganic salts $K_2[B_{12}H_{12}].1CH_3OH$ and $Na_2[B_{12}F_{12}]$ dissolved in water/methanol (1/3 ratio), and the organic salt $[Et_3NH]_2[B_{12}I_{12}]$ dissolved in water/acetonitrile (1/3 ratio) were prepared and sprayed into the gas phase. The hydrated anions were first detected in QMS with their mass intensity distributions tunable by adjusting ESI conditions. The produced hydrated anions were then guided into the cryogenic ion trap (set at 20K) where they were accumulated and cooled by collisions with a cold buffer gas (20% H_2 balanced in He) for 20 – 100 ms, before being pulsed out into the extraction zone of the TOF mass spectrometer for the second mass-to-charge analysis at a repetition of 10 Hz. The hydrated clusters were each mass-selected and decelerated before being photodetached by 193 nm (6.424 eV) or 157 nm photons (7.866 eV) in the interaction zone of the MB photoelectron analyzer. The photodetaching lasers were operated at 20 Hz rate with ion beam off at alternating laser shots to implement shot-to-shot background subtraction. Photoelectrons were collected at nearly 100% efficiency by MB and analyzed in a 5.2-m long calibrated electron flight tube. Recorded electron flight times were converted into kinetic energies. Electron binding energies (EBEs) were obtained by subtracting electron kinetic energies from detachment photon energies used. The energy resolution (ΔE/E) was about 2%, i.e., ∼20 meV full width at half maximum (FWHM) for 1 eV kinetic energy electrons. The experimental vertical detachment energy (VDE) was obtained from the maximum of the lowest EBE band in each spectrum.

Quantum chemical calculations. To obtain global minimum and low-lying isomers of $B_{12}X_{12}^{2-}\cdot H_2O$ (X = H, F, I), a systematic optimization protocol including global semi-empirical quantum mechanical method, density functional theory (DFT), and domain-based local pair natural orbital (DLPNO) coupled-cluster method was performed.[2-9] Initially, 20,000 structures for each $B_{12}X_{12}^{2-}\cdot H_2O$ (X = H, F, I) were generated by the Molclus code.[10] The semiempirical quantum mechanical method GFN2-xTB[11, 12] was employed to optimize the initial geometries in gas phase. A series of energetically low-lying structures were selected and then re-optimized at the PBE0[13]/aug-cc-pVTZ(-pp)[14, 15] level with Grimme's dispersion corrections of GD3BJ.[16, 17] The resulting low-lying isomers were then sorted by high-level DLPNO-CCSD(T)/aug-cc-pVTZ(-pp) method using the ORCA code.[18] The corresponding frequency analyses were performed for lowest-lying structures to ensure that the identified structures are minima on the potential energy surfaces without imaginary frequencies. Gibbs free energies were then calculated with a scale factor of 0.9771[19] for zero-point energy and using quasi-rigid-rotor harmonic oscillator[20] to consider low-frequency contributions at the PBE0/aug-cc-pVTZ(-pp) level utilizing the Shermo code.[21] Finally, the thermal corrected Gibbs free energies at 20 K were included to confirm the most stable configuration. The theoretical vertical detachment energies (VDEs) were determined as the energy differences between the corresponding monoanions and dianions based on the dianion's optimized geometries. Fundamental frequency scaling factor is set to 0.955 in simulating vibrational spectra at the PBE0/aug-cc-pVTZ(-pp) level. The energy decomposition analysis was further performed by the symmetry adapted perturbation theory (SAPT)[22] at the SAPT2+[23]/aug-cc-pVDZ(-pp)[14, 15] level using the PSI4 code.[24] ETS-NOCV analysis, QTAIM and CVB analysis, independent gradient model (IGM) plots and restrained electrostatic potential (RESP) charges were generated by the Multiwfn [25] code and the corresponding isosurfaces were rendered by the VMD program.[26] All DFT calculations were carried out using the Gaussian 16 code.[27]

Ab initio molecular dynamics simulations. Ab initio molecular dynamics (AIMD) simulations were performed using the ORCA 5.0.1 code.[18] The B97-3C/def2-mTZVP method was employed during the AIMD process, considering its good balance between the computational cost and accuracy in describing the noncovalent interactions.[28] A time step of 0.5 fs was set and a time constant of 30 fs was employed for canonical sampling through velocity rescaling (CSVR)[29] to maintain the system temperature. The representative 2000 fs trajectories taken out from a total of 30 ps dynamic trajectories were calculated at different temperatures (20, 30, 40, 50, 60, 70, 100, and 298.15 K). The most stable configuration of each cluster was employed as the initial state and the atom velocities were initialized by the Maxwell-Boltzmann distribution at the corresponding temperatures.

Results and Discussion

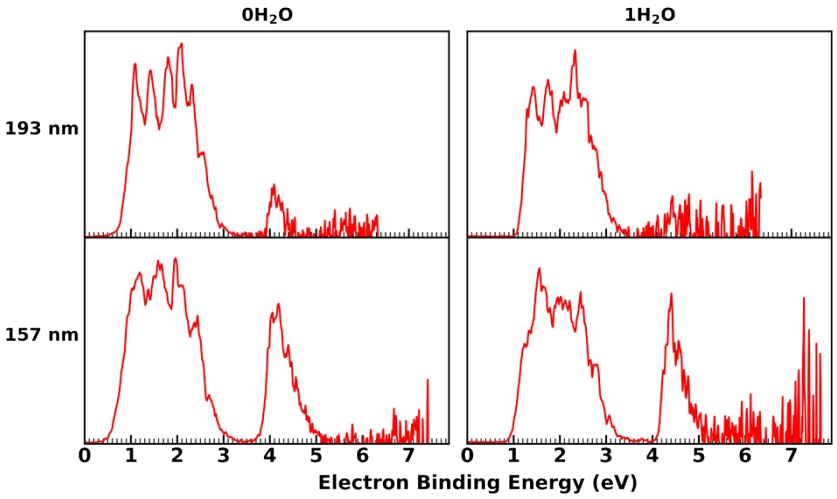

Figure S1. Comparing 20 K 193 nm (6.424 eV) versus 157 nm (7.866 eV) NIPE spectra of $B_{12}H_{12}^{2-}\cdot nH_2O$ (n = 0, 1). A second spectral band with high binding energy shown up at 157 nm is suppressed or completely cut-off by RCB at 193 nm.

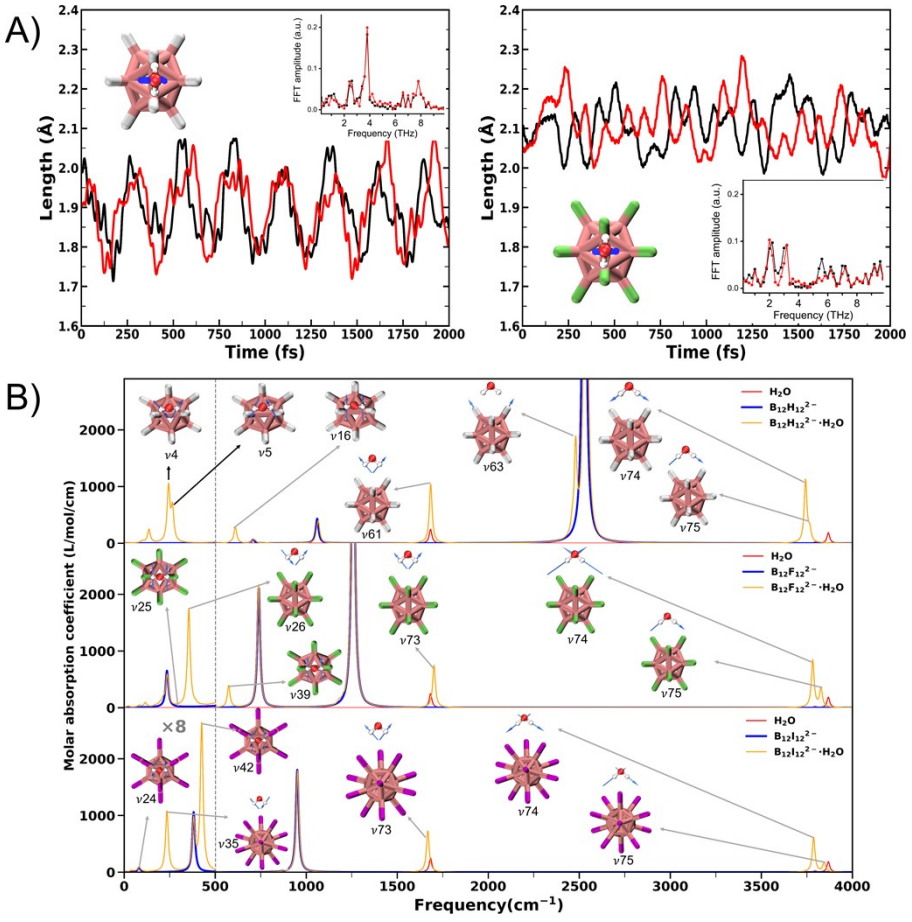

Figure S2. (A) Bond lengths (Å) of two B-H···H-O DHBs in $B_{12}H_{12}^{2-}\cdot H_2O$ and two B-F···H-O HBs in $B_{12}F_{12}^{2-}\cdot H_2O$ as a function of simulation time collected from AIMD trajectories within 2000 fs after equilibrium. (B) Simulated vibrational spectra of $B_{12}X_{12}^{2-}\cdot nH_2O$ (X = H, F, I; n= 0-1) along with the isolated H_2O. Note that the intensity of the infrared peaks under 500 cm^{-1} was amplified eight times (x8).

Assignment	Molecular models			
	$B_{12}H_{12}^{2-}\cdot H_2O$	$B_{12}F_{12}^{2-}\cdot H_2O$	$B_{12}I_{12}^{2-}\cdot H_2O$	H_2O
Plane swing + Non-plane torsion	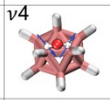			
Plane swing+ Non-plane torsion	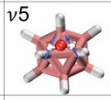			
Non-plane torsion		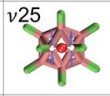	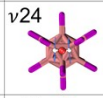	
Plane swing			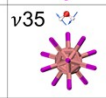	
Non-plane swing	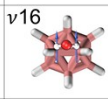	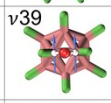	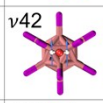	
bend			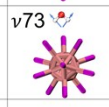	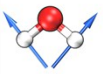
				
Symmetric stretch	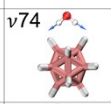	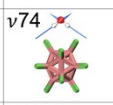	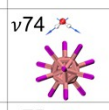	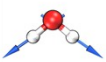
Asymmetric stretch	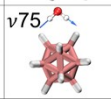	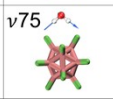	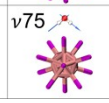	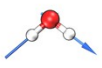

Figure S3. Specific vibrational modes of $B_{12}X_{12}^{2-}\cdot H_2O$ (X = H, F, I) and isolated H_2O.

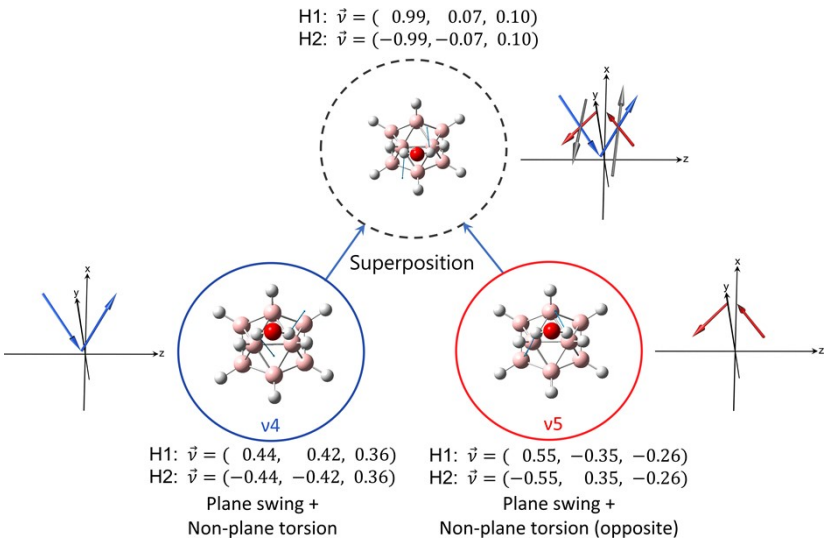

Figure S4. Components of vibrational modes ν_4 and ν_5 for $B_{12}H_{12}^{2-}\cdot H_2O$.

Table S1. Experimental vertical detachment energies (VDEs) and comparison with calculated VDEs using PBE0, DLPNO-CCSD(T), and IP-DLPNO-EOM-CCSD methods with the aug-cc-pVTZ(-pp) basis set for $B_{12}X_{12}^{2-}\cdot nH_2O$ (X = H, F, I; n = 0, 1) (in eV).

	$B_{12}H_{12}^{2-}$	$B_{12}H_{12}^{2-}\cdot H_2O$	$B_{12}F_{12}^{2-}$	$B_{12}F_{12}^{2-}\cdot H_2O$	$B_{12}I_{12}^{2-}$	$B_{12}I_{12}^{2-}\cdot H_2O$
Expt.	1.15	1.46	1.85	2.11	2.80	2.91
DLPNO-CCSD(T)	1.36	1.70	2.07	2.34	2.86	3.05
IP-DLPNO-EOM-CCSD	1.31	1.63	2.03	2.32	3.08	3.18
PBE0	1.29	1.61	1.79	2.07	2.33	2.47

Table S2. Total restrained electrostatic potential charges (RESP charges) of all the B and X atoms in $B_{12}X_{12}^{2-}$ and $B_{12}X_{12}^{2-}\cdot H_2O$ (X = H, F, I) at PBE0/aug-cc-pVTZ(-pp) level.

	$B_{12}H_{12}^{2-}$		$B_{12}F_{12}^{2-}$		$B_{12}I_{12}^{2-}$	
	B	H	B	F	B	I
isolated	0.73	-2.73	2.96	-4.96	-1.32	-0.67
H_2O	0.49	-2.41	2.81	-4.75	-1.61	-0.34

Table S3. The water binding energies (in kcal/mol) for $B_{12}X_{12}^{2-}\cdot H_2O$ (X = H, F, I) calculated by the direct-ΔE and SAPT methods. The ΔZPE and –TΔS (20K) denotes the ZPE and entropic correction, respectively, and the corresponding contribution to ΔE were shown in parentheses.

	$B_{12}H_{12}^{2-}\cdot H_2O$	$B_{12}F_{12}^{2-}\cdot H_2O$	$B_{12}I_{12}^{2-}\cdot H_2O$
Direct ΔE	-12.264	-11.447	-9.762
ΔZPE	0.244 (2.0%)	0.287 (2.5%)	0.262 (2.7%)
-TΔS	1.941 (1.6%)	1.936 (1.7%)	1.145 (1.2%)
SAPT	-14.308	-13.164	-8.737

Table S4. (a) Calculated quantum theory of atoms in molecules (QTAIM) topological descriptors at the bond critical point (BCP) of (D)HBs and other core-valence bifurcation (CVB) indices for the studied complexes.

	QTAIM index					CVB index
	ρ(r)	H(r)	$\nabla^2\rho(r)$	H(r)/ρ(r)	|V(r)|/G(r)	ELF(C-V)
	(a.u.)	(a.u.)	(a.u.)			(a.u.)
$B_{12}H_{12}^{2-}\cdot H_2O$	0.017	0.00026	0.041	0.016	0.974	0.0882
$B_{12}F_{12}^{2-}\cdot H_2O$	0.019	0.00213	0.076	0.112	0.874	0.0878
$B_{12}I_{12}^{2-}\cdot H_2O$	0.007	0.00058	0.018	0.095	0.830	0.0868

ρ(r): density of all electrons, the value of ρ(r) at BCP are closely related to bonding strength and bonding type respectively for analogous bonds (*J. Comput. Chem. 2019, 40, 2868*).
H(r): electronic energy density, the negative and positive values imply the bond has covalent and non-covalent nature, respectively (*Angew. Chem. Int. Ed., 1984, 23, 627*).
$\nabla^2\rho(r)$: Laplacian of electron density at BCP, negative and positive values imply that the major nature of the bond is covalent and non-covalent, respectively (*J. Comput. Chem. 2019, 40, 2868*).
H(r)/ρ(r): The physical meaning denotes energy density of unit electron at BCP, negative and positive values imply that the major nature of the bond is covalent and non-covalent, respectively. (*J. Chem. Phys.*, 2002, 117, 5529)
|V(r)|/G(r): the ratio of absolute potential energy density |V(r)| to Lagrangian kinetic energy density G(r) at BCP. The bonding mainly belongs to close-shell interaction (< 0) and intermediate (0 ~ 2) interaction and covalent interaction (> 2) (*J. Chem. Phys.*, 2002, 117, 5529).
ELF(C-V): the electron localization function (ELF) bifurcation value between ELF core domain and valence domain (*J. Chem. Phys. 1990, 92, 5397*).

(b) schematic diagram of the bond critical point (BCP) of (D)HBs

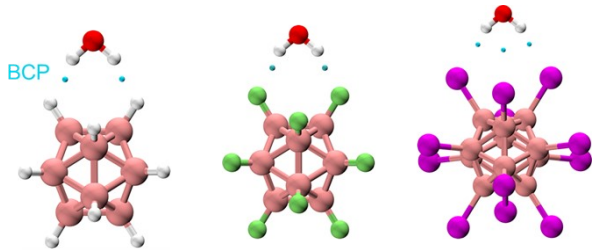

$B_{12}H_{12}^{2-}\cdot H_2O$ $B_{12}F_{12}^{2-}\cdot H_2O$ $B_{12}I_{12}^{2-}\cdot H_2O$

Table S5. (A) Energy decomposition analysis (EDA) of different components (in kcal/mol) for $B_{12}X_{12}^{2-}\cdot H_2O$ (X = H, F, I) calculated at SAPT2+/aug-cc-pVDZ(-pp) level. (B) The differences of each EDA term of $B_{12}X_{12}^{2-}\cdot H_2O$ (X = F, I) relative to the respective term of $B_{12}H_{12}^{2-}\cdot H_2O$. The attractions and repulsion terms were converted to positive and negative values in Figure 3.

(A)	$B_{12}H_{12}^{2-}\cdot H_2O$	$B_{12}F_{12}^{2-}\cdot H_2O$	$B_{12}I_{12}^{2-}\cdot H_2O$
Electrostatic (Elst.)	-16.578	-16.057	-9.877
Exchange (Exch.)	12.141	11.073	8.206
Induction (Ind.)	-4.736	-3.883	-2.501
Dispersion (Disp.)	-5.136	-4.297	-4.564
(B)	$B_{12}H_{12}^{2-}\cdot H_2O$	$B_{12}F_{12}^{2-}\cdot H_2O$	$B_{12}I_{12}^{2-}\cdot H_2O$
ΔElst.	0	-0.521	-6.701
ΔExch.	0	1.068	3.935
ΔInd.	0	-0.852	-2.234
ΔDisp.	0	-0.839	-0.571
Total ΔBE	0	-1.144	-5.571

Table S6. Frequencies (in cm^{-1}) and transition intensities (km/mol) of the selected vibrational modes in $B_{12}X_{12}^{2-}\cdot H_2O$ (X = H, F, I) and isolated H_2O.

$B_{12}H_{12}^{2}\cdot H_2O$			$B_{12}F_{12}^{2}\cdot H_2O$			$B_{12}I_{12}^{2}\cdot H_2O$			H_2O		
Mode	Freq./ cm^{-1}	I_{IR}/ km/mol	Mode	Freq./ cm^{-1}	I_{IR}/ km/mol	Mode	Freq./ cm^{-1}	I_{IR}/ km/mol	Mode	Freq./ cm^{-1}	I_{IR}/ km/mol
***ν*4**	232.7	34.3									
***ν*5**	253.3	20.1									
			***ν*25**	323.6	0.0	***ν*24**	81.3	1.2			
			***ν*26**	339.1	60.9	***ν*35**	224.4	37.7			
***ν*16**	583.1	81.7	***ν*39**	548.4	108.9	***ν*42**	406.7	92.0			
***ν*61**	1608.3	295.8	***ν*73**	1625.5	210.7	***ν*73**	1593.1	205.7	***ν*1**	1607.4	70.2
***ν*63**	2368.6	445.4									
***ν*74**	3574.8	313.0	***ν*74**	3612.5	236.2	***ν*74**	3617.0	172.5	***ν*2**	3624.6	5.6
***ν*75**	3596.8	57.0	***ν*75**	3655.9	94.2	***ν*75**	3672.4	47.8	***ν*3**	3694.3	52.6

References

1. X.-B. Wang and L.-S. Wang, *Rev. Sci. Instrum.*, 2008, **79**, 073108.

2. F. Neese, A. Hansen and D. G. Liakos, *J. Chem. Phys.*, 2009, **131**, 064103.
3. F. Neese, A. Hansen, F. Wennmohs and S. Grimme, *Acc. Chem. Res.*, 2009, **42**, 641-648.
4. F. Neese, F. Wennmohs and A. Hansen, *J. Chem. Phys.*, 2009, **130**, 114108.
5. A. Hansen, D. G. Liakos and F. Neese, *J. Chem. Phys.*, 2011, **135**, 214102.
6. D. G. Liakos, A. Hansen and F. Neese, *J. Chem. Theory Comput.*, 2011, **7**, 76-87.
7. L. M. J. Huntington, A. Hansen, F. Neese and M. Nooijen, *J. Chem. Phys.*, 2012, **136**, 064101.
8. C. Riplinger and F. Neese, *J. Chem. Phys.*, 2013, **138**, 034106.
9. C. Riplinger, B. Sandhoefer, A. Hansen and F. Neese, *J. Chem. Phys.*, 2013, **139**, 134101.
10. T. Lu, Molclus program, http://www.keinsci.com/research/molclus.html).
11. C. Bannwarth, S. Ehlert and S. Grimme, *J. Chem. Theory Comput.*, 2019, **15**, 1652-1671.
12. M. Bursch, H. Neugebauer and S. Grimme, *Angew. Chem., Int. Ed.*, 2019, **58**, 11078-11087.
13. C. Adamo and V. Barone, *J. Chem. Phys.*, 1999, **110**, 6158-6170.
14. R. A. Kendall, T. H. Dunning and R. J. Harrison, *J. Chem. Phys.*, 1992, **96**, 6796-6806.
15. K. A. Peterson, B. C. Shepler, D. Figgen and H. Stoll, *J. Phys. Chem. A*, 2006, **110**, 13877-13883.
16. S. Grimme, J. Antony, S. Ehrlich and H. Krieg, *J. Chem. Phys.*, 2010, **132**, 154104.
17. S. Grimme, S. Ehrlich and L. Goerigk, *J. Comput. Chem.*, 2011, **32**, 1456-1465.
18. F. Neese, *WIREs Computational Molecular Science*, 2018, **8**, e1327.
19. J. P. Merrick, D. Moran and L. J. T. j. o. p. c. A. Radom, 2007, **111 45**, 11683-11700.
20. S. Grimme, *Chemistry – A European Journal*, 2012, **18**, 9955-9964.
21. T. Lu and Q. Chen, *Computational and Theoretical Chemistry*, 2021, **1200**, 113249.
22. B. Jeziorski, R. Moszynski and K. Szalewicz, *Chem. Rev.*, 1994, **94**, 1887-1930.
23. E. G. Hohenstein and C. D. Sherrill, *J. Chem. Phys.*, 2010, **133**, 014101.
24. R. M. Parrish, L. A. Burns, D. G. A. Smith, A. C. Simmonett, A. E. DePrince, E. G. Hohenstein, U. Bozkaya, A. Y. Sokolov, R. Di Remigio, R. M. Richard, J. F. Gonthier, A. M. James, H. R. McAlexander, A. Kumar, M. Saitow, X. Wang, B. P. Pritchard, P. Verma, H. F. Schaefer, K. Patkowski, R. A. King, E. F. Valeev, F. A. Evangelista, J. M. Turney, T. D. Crawford and C. D. Sherrill, *J. Chem. Theory Comput.*, 2017, **13**, 3185-3197.
25. T. Lu and F. Chen, *J. Comput. Chem.*, 2012, **33**, 580-592.
26. W. Humphrey, A. Dalke and K. Schulten, *J. Mol. Graph.*, 1996, **14**, 33-38.
27. M. J. Frisch, G. W. Trucks, H. B. Schlegel, G. E. Scuseria, M. A. Robb, J. R. Cheeseman, G. Scalmani, V. Barone, G. A. Petersson, H. Nakatsuji, X. Li, M. Caricato, A. V. Marenich, J. Bloino, B. G. Janesko, R. Gomperts, B. Mennucci, H. P. Hratchian, J. V. Ortiz, A. F. Izmaylov, J. L. Sonnenberg, Williams, F. Ding, F. Lipparini, F. Egidi, J. Goings, B. Peng, A. Petrone, T. Henderson, D. Ranasinghe, V. G. Zakrzewski, J. Gao, N. Rega, G. Zheng, W. Liang, M. Hada, M. Ehara, K. Toyota, R. Fukuda, J. Hasegawa, M. Ishida, T. Nakajima, Y. Honda, O. Kitao, H. Nakai, T. Vreven, K. Throssell, J. A. Montgomery Jr., J. E. Peralta, F. Ogliaro, M. J. Bearpark, J. J. Heyd, E. N. Brothers, K. N. Kudin, V. N. Staroverov, T. A. Keith, R. Kobayashi, J. Normand, K. Raghavachari, A. P. Rendell, J. C. Burant, S. S. Iyengar, J. Tomasi, M. Cossi, J. M. Millam, M. Klene, C. Adamo, R. Cammi, J. W. Ochterski, R. L. Martin, K. Morokuma, O. Farkas, J. B. Foresman and D. J. Fox, *Journal*, 2016.
28. J. G. Brandenburg, C. Bannwarth, A. Hansen and S. Grimme, *J. Chem. Phys.*, 2018, **148**, 064104.
29. G. Bussi, D. Donadio and M. Parrinello, *J. Chem. Phys.*, 2007, **126**, 014101.